ΔΗΜΟΣ ΚΟΝΙΤΣΑΣ
Ο τόπος των πέτρινων γεφυριών

Κόνιτσα 11/01/2019

ΔΕΛΤΙΟ ΤΥΠΟΥ

ΕΠΙΣΤΗΜΟΝΙΚΟ ΑΡΘΡΟ ΓΙΑ ΤΗΝ ΑΡΧΙΤΕΚΤΟΝΙΚΗ ΑΞΙΑ ΤΩΝ ΠΑΡΑΔΟΣΙΑΚΩΝ ΓΕΦΥΡΙΩΝ ΤΗΣ ΚΟΝΙΤΣΑΣ

Τα Μαστοροχώρια του Δήμου Κόνιτσας στους πρόποδες του Γράμμου, φημίζονται για τους ικανούς μαστόρους και την ξεχωριστή μαστορική τέχνη, που άφησε ανεξίτηλα και διαχρονικά σημάδια με τα λιτά, πέτρινα κτήρια και τα μοναδικά γεφύρια, αφού η φήμη των μαστόρων είχε εξαπλωθεί τόσο στην Ελλάδα, όσο και σε όλο τον κόσμο.

Αυτή η τέχνη της περιοχής, καθώς και η αρχιτεκτονική αξία του μονότοξου, λίθινου γεφυριού της Κόνιτσας προβάλλεται και αναδεικνύεται σε παγκόσμιο επίπεδο, σε άρθρο στο επιστημονικό περιοδικό ***Engineering Structures*** (www.elsevier.com/locate/engstruct) του συμπατριώτη μας Νικόλαου Σίμου, επίτιμου καθηγητή στο BNL's Collider Accelator Department and the National Synchrotron Light Source II (NSLS II) και των επιστημόνων - καθηγητών Γιώργου Μάνου και Ευάγγελου Κοζικόπουλου, τους οποίους και ευχαριστούμε θερμά.

Ακολουθεί το σχετικό άρθρο:

Engineering Structures 177 (2018) 256–267

Contents lists available at ScienceDirect

Engineering Structures

journal homepage: www.elsevier.com/locate/engstruct

Near- and far-field earthquake damage study of the Konitsa stone arch bridge

Nikolaos Simos[a,*], George C. Manos[b], Evaggelos Kozikopoulos[b]

[a] Brookhaven National Laboratory, USA
[b] Laboratory of Experimental Strength of Materials and Structures, Department of Civil Engineering, Aristotle University of Thessaloniki, Greece

ARTICLE INFO

Keywords:
Stone arch bridge
Finite element analysis
Seismic response
Earthquake vulnerability

ABSTRACT

This paper reports on the sensitivity of earthquake response and damage of long span masonry stone bridges to near field (impulsive type) and far field earthquakes. Towards that objective, the Konitsa Bridge is used as a case study. The particular bridge was selected for offering certain unique features such as long span, built right on an active fault, survived a recent pair of near-filed type earthquakes with minimal damage and finally, construction material mechanical properties and strength could be deduced from a recently collapsed similar bridge in the area. The multifaceted study integrated in-situ measurements of dynamic characteristics, laboratory tests on representative stone and mortar materials and a series of finite-element analyses based on non-linear modelling using a combination of discontinuous and continuous representations to capture the behavior of bridge structural component interface and interaction as well as mortar-stone interaction and failure. In addition to the ground motion records of the recent seismic activity at the Konitsa Bridge location, four additional earthquake records representing near-field and far-field families were utilized to assess the stone bridge sensitivity. The study revealed that far-field earthquakes are far more destructive than near-field counterparts, a finding in full agreement with studies on near field earthquake effects on nuclear structures. The applicability of earthquake damage indicators such as CAV, Arias intensity and energy rate, typically used for conventional and nuclear structures, was evaluated based on the numerical analysis results.

1. Introduction

Masonry arch bridges are an integral component of the heritage of cultures worldwide reflecting unique engineering techniques developed over the centuries characterizing the region where they are located. Typically, masonry stone bridges were constructed to serve local communities by utilizing construction materials from the vicinity and therefore allowing the construction techniques to evolve and adopt to the quality of the available raw materials. Due to ageing, neglect and compounded with often poor-quality restoration works that were performed on these structures over the years there is an urgent need to evaluate their current structural health state, identify structural degradation and locations of distress and perform appropriate restoration based on sound engineering assessment. The unique engineering techniques used in the construction of these bridges poses a challenging engineering problem and an intriguing numerical case for predicting their dynamic response and seismic vulnerability.

In the last couple of decades experimental and numerical studies on masonry stone bridges have been performed to address both the ageing as well as the impact of vehicle or rail traffic both of which were not accounted for in the original construction. T. Akoi and co-workers [1] studied the Rakanji Bridge in Japan. Most relevant in this study is the fact that study conducted both stone and mortar tests establishing a good basis of analysis and material properties. Both micro-tremor measurement by ambient vibrations and acceleration by traffic vibrations were measured. Laboratory tests on similar materials to those of the bridge were conducted to establish the Young's modulus and compressive strength of the stone and the mortar. A number of historic stone arched bridges around Japan were studied by J. Kiyono and his co-workers [2]. In their all numerical study the dynamic behavior of several stone arched bridges were simulated using the 3-dimentional Distinct Element Method. Actual earthquake ground motions observed during the 1995 Hyogo-ken Nanbu earthquake were used in their study in conjunction with impulse waves to determine the modal characteristics and their collapse potential. G. Castellazzi and co-workers [3] conducted 3D finite element modelling and in situ experimental testing. To deduce both the material properties of the masonry constituting and the structural behavior of a masonry case study bridge subjected to

* Corresponding author.
E-mail address: simos@bnl.gov (N. Simos).

https://doi.org/10.1016/j.engstruct.2018.09.072
Received 14 July 2016; Received in revised form 30 August 2018; Accepted 24 September 2018

increased rail traffic. L. Pelà et al. [5] studied the seismic performance of existing masonry arch bridges using non-linear techniques and following procedures and standards including pushover analyses and response spectrum approaches. Laboratory tests were also conducted to aid the calibration of their model. Seismic assessment and retrofitting measures of a historic stone masonry bridge that experienced a M7.2 earthquake in1953 and recent M6.1 and M6.0 earthquakes in 2014 was studied in [6] in a parametric study to reverse poorly-designed and implemented restorations. B. Sevim and co-workers [7,8] conducted studies of arch bridges in Turkey where ambient vibration data were utilized to calibrate numerical models which subsequently were used to conduct earthquake analyses of stone arch bridges by representing the stone/mortar elements as a linear elastic homogeneous continuum. In [8] the response of bridges under near and far fault ground motions have been calculated using linear finite element analysis and, according to the authors [8], near fault ground motions impose higher seismic demand on the arch, an assessment derived from calculated higher displacements and stresses. Findings in [8] are contrary to a wealth of reported experimental and analytical data on nuclear-type structures [29–31] as well as experience data from sitting of nuclear reactor installations where near-field earthquakes of magnitude $M \leq 5.5$ have been treated as low damageability potential earthquakes [29], It should be emphasized, however, that the linear-elastic treatment of the arch bridge structures in [8] may very well produce higher displacements and subsequently stresses when subjected to a near-field earthquake signal due to the presence of a dominant velocity pulse that characterizes near-field earthquakes.

A large body of research work has been reported in recent years [4,9–14] aiming to characterize the complex mechanical behavior of the two-material system (stone and mortar) and deduce constitutive relations as well as failure behavior. Objective of this body of research was the combining the properties of the “unit block” (stone) exhibiting high compressive strength with the mortar which exhibits brittle behavior in tension and governed by friction in shear. Computational strategies for masonry structures were addressed in a PhD Thesis [4] by J. B. Lourenço. The anisotropy of the material is such that a complete description is impossible and therefore simplifications must be made. In [14] Drosopoulos and co-workers studied the ultimate failure load of stone arch bridges based on 2-D, plane strain finite element analysis which included interfaces, simulation of cracks, unilateral friction contacts and the implementation of a path-following technique to estimate the ultimate load. Comparison to relevant experimental results was also presented. Numerical techniques addressing the interaction of mortar and stone blocks or block-block non-linear contact were also explored. Specifically, B. O. Caglayan and co-workers [15] integrated a 3-D finite element analysis with in-situ acceleration measurements to study a long concrete arch bridge located in an earthquake-prone region. Structural analysis of masonry historical constructions were conducted in [16] based on limit analysis, simplified methods, FEM macro- or micro-modeling and discrete element methods (DEM). Numerical analyses [17–20] based on 3D non-linear finite elements were used to study masonry structures and in particular stone bridges. Results of a comprehensive assessment of the case study (Konitsa Bridge) are presented in [21]. Seismic hazards associated with the region and practices are presented in [22–28]. The effects of near-field and far field earthquakes on nuclear structures based on shake table experiments and confirmatory numerical studies are presented in [29–31]. Damage indicators of earthquakes used in seismic vulnerability assessment and field observations, including correlation with observed damage, are discussed in [32,33]. Observations and studies of masonry structures under seismic loads are reported in [34–39,41–43].

In the present study a 3D, non-linear analysis of a large arch stone bridge was performed as a case study for assessing the damageability of different type of earthquakes, i.e. near-field and far-field, on these structures. The selection of the Konitsa Bridge as the reference structure was prompted by the fact that it is situated on a known fault, its performance/survivability to a pair of recent near field earthquakes was assessed plus the fact that actual seismic ground motions were recorded in the proximity of the bridge. Furthermore, the recent collapse of a similar large stone arch bridge in the general area, built at the same period (1870) with similar material and techniques provided access to actual aged structural materials (mortar in particular) for laboratory testing and eventual use of the test data in the case study bridge. Using the non-linear capabilities of the LS-DYNA finite element code a numerical representation of the bridge was deduced as combination of discontinuous model (between distinct structural sections such as primary arch and secondary arch or mandrel wall) and continuous model (within each structural section). Specifically, interface conditions and failure between structural segments are governed by the mortar failure behavior. In the “continuous model” the governing constitutive relations and failure characteristics of a “unit” or element representing the stone-mortar materials and their interaction are those of a Winfrith type concrete with two-phase material where the mortar is smeared within the unit or element. Tension cracking is assumed to be controlled by mortar while crushing by the stone material. Properties from the laboratory tests were used in the adopted constitutive relations and failure. Two independent campaigns were conducted on the case bridge to deduce modal and damping characteristics and help fine-tune the numerical model. Sought in the main body of the current research reported within, is the structural damage sensitivity of this case study structure (and others like it) to the nature or type of near-field and far-filed earthquake motions. Actual earthquakes recorded around the world were utilized and the predicted damage, as well as the applicability of metrics of earthquake damage potential used in modern earthquake engineering (i.e. CAV, Arias Intensity) are assessed. The studies revealed, that the damageability of far-field earthquakes is more severe than that of near-field counterparts of same peak ground acceleration, in agreement with findings of experimental studies on nuclear-type structures [30].

2. Case study bridge location and structural characteristics

2.1. Location and structural details

The case study Konitsa Bridge shown in Fig. 1 was built in 1870 and is located at the mouth of the Aoos River Gorge near the city of Konitsa, northwestern Greece. It is in close proximity to the Konitsa fault (Fig. 2) and, following the recent collapse of the Plaka Bridge [19], is the largest of its kind single arch stone bridge in Greece. Approximately twenty (20) single arch stone bridges with arch opening > 12 m are found in north-western Greece. It is of significant cultural heritage value as it represents the stone building art of the wider region. It is a single span structure made from natural, local stone with a primary (lower) and secondary (upper) arches. It has an opening of 39.8 m, height of 20 m. The primary arch has a thickness of 1.30 m and the secondary arch a thickness of 0.59 m. The deck width is 3 m with a protective parapet. It is not clear, however, as to width and thus weight of the original construction parapet and whether the one currently in place represents the original construction (poor quality restoration work was performed between 1988 and 1992). It also evident that during this structural intervention “restoration” was also performed in critical elements of the bridge (sections of the lower and upper arches near the crown as shown in Fig. 1) where concrete replaced the stone work and a steel mesh was introduced in part of the intrados. Important structural features to note are (a) the “periodical” tie keys which have been used in long span stone bridges of the region and (b) the geometric configuration of the abutment stone layers receiving the normal load from the ends of two arches that they support (Fig. 1c; d). As shown in Fig. 1 the LHS abutment foundation is supported on rock base while the RHS abutment on foundation that is embedded in what appears to be “weathered” rock. Details on the depth of the RHS foundation are not readily available and therefore uncertainties of whether a competent

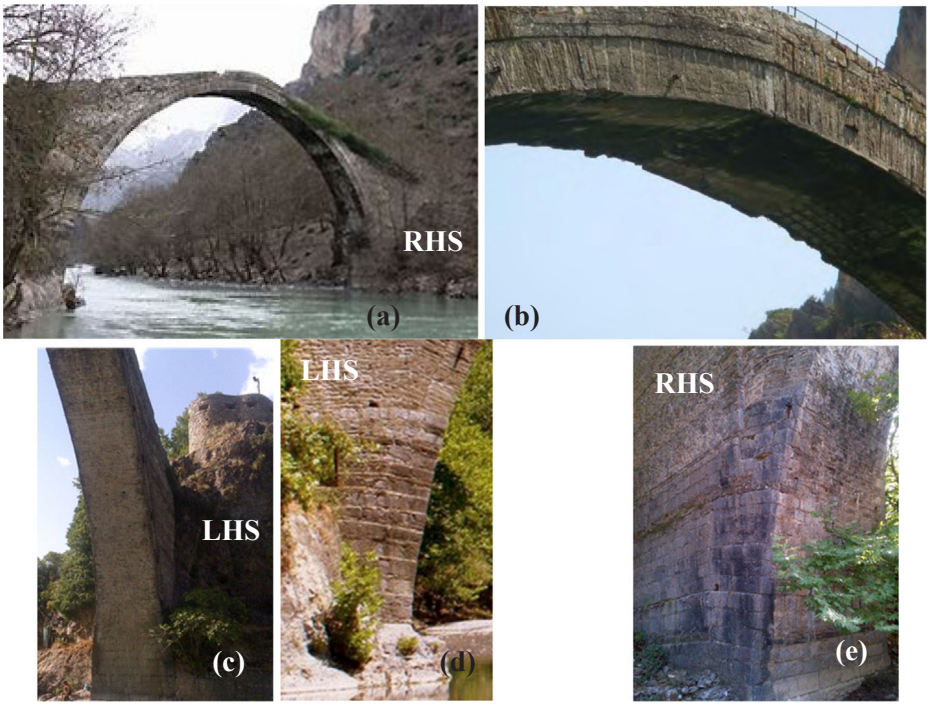

Fig. 1. (a) General view, (b) primary arch restoration including steel mesh addition, (c–d) LHS abutment foundation, and (e) RHS abutment foundation details of the Konitsa Bridge.

rock is supporting the RHS abutment persist. Such detail could have engineering significance in that the earthquake excitation would exhibit differences between the two supports.

2.2. Area seismic hazards

According to seismological hazard studies [22–24] the immediate area of Konitsa does not present strong seismicity. It has, however, experienced destructive earthquakes in the past with magnitudes M > 6.0 and epicenters at considerable distances from the location of the bridge and therefore can be considered as far-field earthquakes. The so called Konitsa fault (Fig. 2) which constitutes the main neo-tectonic structure in the proximity of the bridge is too close for comfort for the structure. The most recent earthquake in the proximity of the Konitsa Bridge occurred in August 1996. The epicenter of the 6th August earthquake (M = 5.7) with 8 km depth was about 15 km to the SW of the bridge. While no recording at the bridge location is available, the earthquake was recorded at less than a kilometer away on soft soil with maximum acceleration of 0.39 g [23]. A similar recording on rock (~1.5 Km away and on the same rock formation to that supporting the LHS buttress of the Konitsa Bridge) indicated a peak ground acceleration of 0.19 g. During the 1996 earthquake limited damage was experienced by the bridge in the form of (a) spalling of the protective cement layer in the bridge intrados, (b) loss of parapet sections and (c) few tension cracks on RHS abutment.

2.3. Bridge modal characteristics – field studies

To gain a good understanding of the current state of the bridge, and in addition aid the fine-tuning of the numerical model that is to be used in the earthquake damage analyses, two (2) independent field studies based on two different measurement apparatus were conducted to

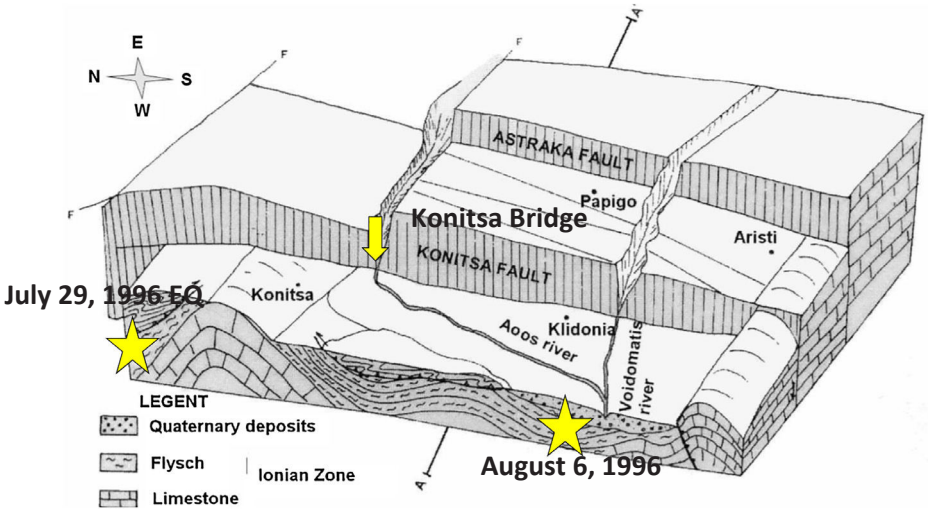

Fig. 2. Konitsa Bridge location relative to local major faulting and most recent earthquake source locations (reproduced from Galanakis et al. [23]).

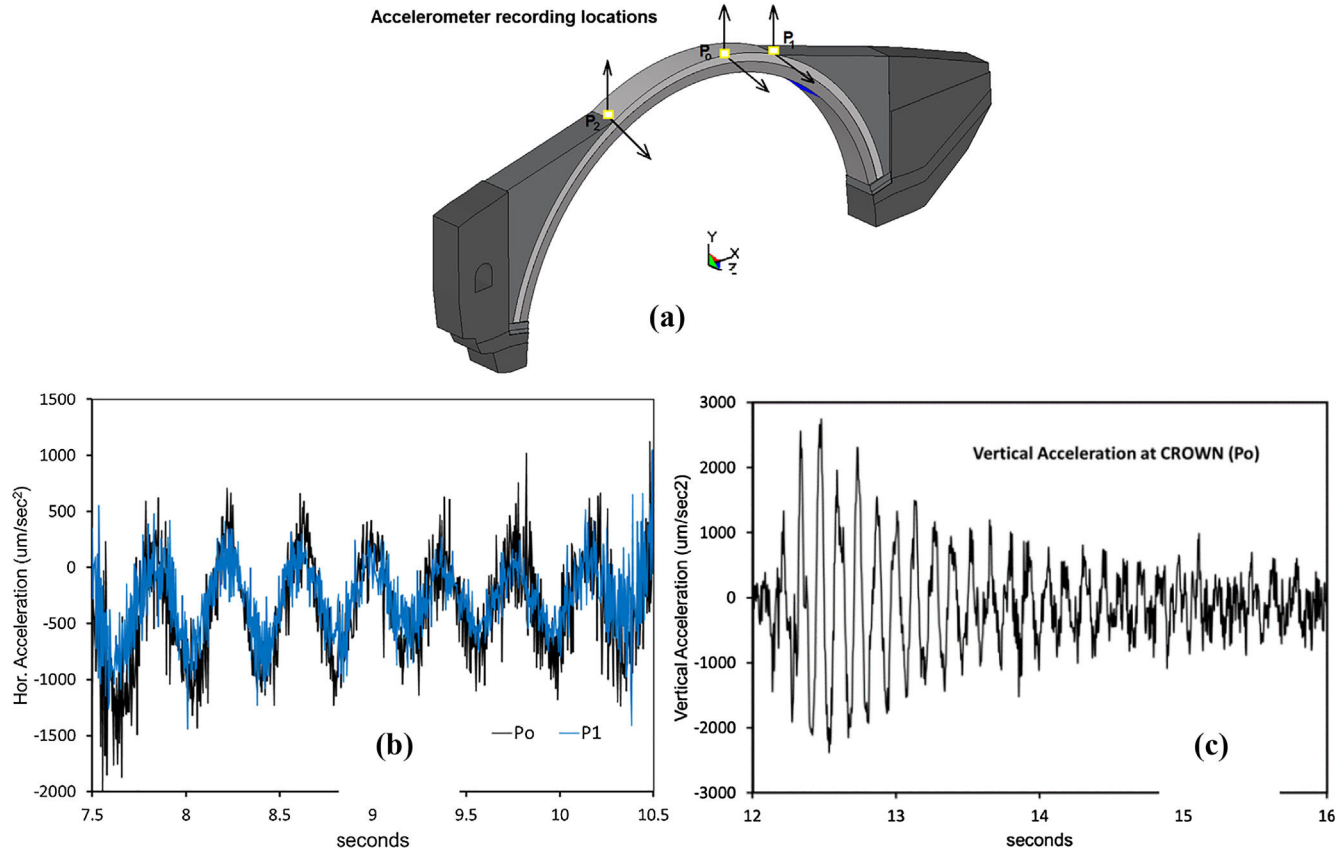

Fig. 3. (a) Sensor locations, (b) out of plane and (c) vertical acceleration time history segments recorded on the Konitsa Bridge deck during post-wind gust decay.

deduce the dynamic characteristics of the structure (vibrational modes and damping). Ambient vibrations, transients and long averaged spectra, as well as response to external excitations (wind gusts and drop weights) were captured and analyzed. Measurements included acceleration time histories and corresponding Fourier spectra, long-term averaged Fourier spectra, coherence measurements and transfer function characteristics of the structure. The field study focused primarily on the out of plane and vertical motion directions which are dominate the bridge response. Fig. 3a depicts the measuring locations and accelerometer directions on the bridge deck. Shown in Fig. 3b are transient horizontal accelerations captured simultaneously at two locations on the bridge deck and in Fig. 3c transient vertical acceleration at crown. The decaying acceleration amplitude recorded used in estimating damping based on the relation $\ln(x/x_m) = 2\pi\,\delta\, m/\sqrt{1-\delta^2}$ over the decay segment of the recording the damping ratio estimated is of ~1.6%.

Fig. 4 depicts long averaged recorded spectra in the out of plane (horizontal) and in-plane (vertical) directions. Fig. 5 depicts damping estimation based on induced oscillation "decay" measurements from the second field campaign. The in-plane excitations of the second campaign were induced by a 2.0 kN weight dropped from a height of 100 mm was used. The two campaigns deduced similar dynamic characteristics of the bridge both in terms of bridge characteristic frequencies and damping. The identified Konitsa bridge frequencies from the recorded data are listed in Table 1.

As depicted in Fig. 4 and Table 1, the main symmetric out-of-plane vibration that is excited by the wind has a dominant period of 2.563 Hz and a corresponding damping ratio ~1.7%. The main symmetric in-plane vibration exhibits a dominant period of 7.715 Hz and a corresponding damping ratio approximately 2.7%. This increase in the damping ratio value may be attributed to the relatively larger amplitudes of vibration produced by the drop weight as compared to those from wind gust excitation. Decay characteristics from induced oscillations used for damping estimation are shown in Fig. 5.

3. Numerical (FE) model generation

3.1. Material properties

Construction material properties (natural stone and mortar) of bridge structures are expected to vary from region to region influenced by the variation of the natural materials available in the immediate locality. Such variability is primarily expected to impact the mortar used (composition, weathering, mechanical properties, etc.) and consequently the overall response of the structure. The recent collapse of the Plaka Bridge [19], which as noted previously was constructed around the same period, with same techniques and materials, offered the opportunity to study actual, weathered materials (stone and mortar) retrieved from the collapsed structure in the laboratory. The results of the lab tests provide a good estimate of the material strength and properties required as input to the seismic study of the Konitsa Bridge. Test specimens of stone and mortar of regular prismatic geometry were extracted and tested at the laboratory of Strength of Materials and Structures of Aristotle University, Thessaloniki, Greece. The test specimens were subjected to axial compression as well as four-point bending by employing load cells to measure the applied load and a combination of displacement sensors as well as several strain gauges to measure the resulting deformation with 10 Hz sampling frequency. Two prismatic samples were used for stone compression tests of sizes 61 mm × 68 mm × 93 mm and 67.5 mm × 62 mm × 89 mm respectively. For the stone flexure tests two specimens with a span of 180 mm and a cross sectional area of 52 × 52 mm^2 were used. The mortar samples used in the compression and flexure tests had a cross sectional area of 27.5 × 57 mm^2 and 66 mm length.

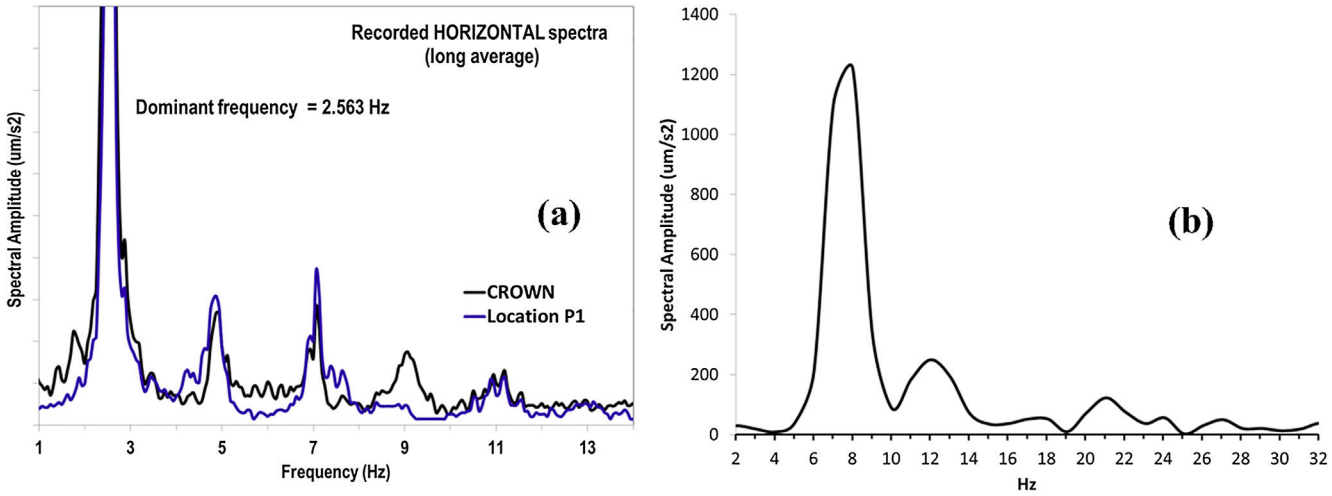

Fig. 4. (a) Horizontal and (b) vertical spectra (averaged) from long-term measurements.

Compression tests revealed an average of 71.3 MPa in stone compression strength, a Poisson's ratio ν of 0.142 and modulus E_1 of 40 GPa (E_1 represents the Young's modulus deduced from compression tests). For the compression tests the reference slenderness ratio was equal to 2.0 and the average compressive strength refers to a prism with slenderness ratio of 2.0. Stone flexure tests led to an average tensile strength of 17.20 MPa and modulus $E_2 \sim 34.8$ GPa (E_2 represents the Young's modulus deduced from flexure tests). The stone direct tensile strength of ~6.5 MPa has been deduced from the flexure tensile strength by using a conservative flexural/tensile factor of ~0.38. The average mortar tensile strength from flexure was found to be ~1.267 MPa whereas the mortar average compressive strength was ~10.275 MPa. Conservative estimates of the mortar direct tensile strength have been made using factors as low as 0.33 leading to strength values of 0.42 MPa. The mortar modulus was estimated to be $E_{mortar} \sim 2500$ MPa and the Poisson's ration $\nu = 0.35$.

Testing of rock-like materials has been conducted by Prof. L. Biolzi and co-workers [40] where bending strengths are compared with the direct strength from double-edge-notched specimens of medium grained size granite. Techniques such as electronic speckle pattern interferometry and acoustic emission, in addition to direct tensile and the standard compression and three-point-bending tests, were integrated to capture the evolution of cracking and displacement fields. It was assessed in [40] that the flexural/tensile strength ratio for the tested medium grain-size granite depends strongly on the microstructure and the specimen size. In fitting the experimental data [40] flexural/tensile ratios of ~0.75 were deduced. However, due to the differences in the microstructure of the stone and the mortar, as compared to the granite tested in [40], the authors believe that the more conservative factor values 0.38 and 0.33 respectively used are more appropriate for the present study.

No attempt was made during this test phase to measure the bond strength between stone and mortar. The mortar direct tensile strength has been assumed as an upper limit of the bond strength between the two materials in the numerical studies.

Table 1
Konitsa Bridge measured modes.

Out-of-plane modes (OOP)		In-plane modes (IP)	
1st OOP symmetric:	2.563 Hz	1st IP asymmetric:	5.176 Hz
2nd OOP asymmetric:	4.883 Hz	2nd IP symmetric:	7.715 Hz
3rd OOP symmetric:	7.129 Hz	3rd IP symmetric:	12.549 Hz
4th OOP asymmetric:	9.326 Hz		

3.2. Constitutive models and failure of the interfaces

The numerical scheme adopted in the analysis to emulate constitutive and failure (cracking and or crushing) relations in the stone-mortar system consists of both "discontinuous" and "continuous" representations [45]. The "discontinuous" representation or failure criteria are implemented between distinct structural sections of the stone bridge (i.e. interface of primary arch with the secondary arch or abutments, etc.) and the "continuous" representation implemented within each structural segment (i.e. stone and mortar non-linear behavior within the primary arch or within the abutments, the mandrel walls, etc.)

Shown in Fig. 6 are the two strategies implemented in the present study to emulate the non-linear behavior and failure in the structure. Fig. 6a reveals the discontinuous discretization of the structure into distinct sections which interface with each other through non-linear contact whose non-linear behavior and failure is controlled by the properties and strength of the mortar layer that exists over these interfaces between distinct structural sections. It is the belief of the authors that such description adheres closely to the actual construction of these type of stone structures. A constitutive interface model

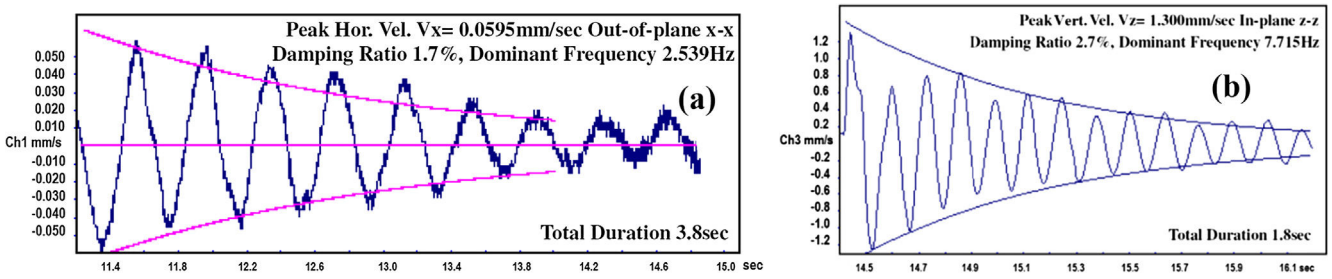

Fig. 5. Induced oscillation "decay" measurements, (a) horizontal and (b) vertical.

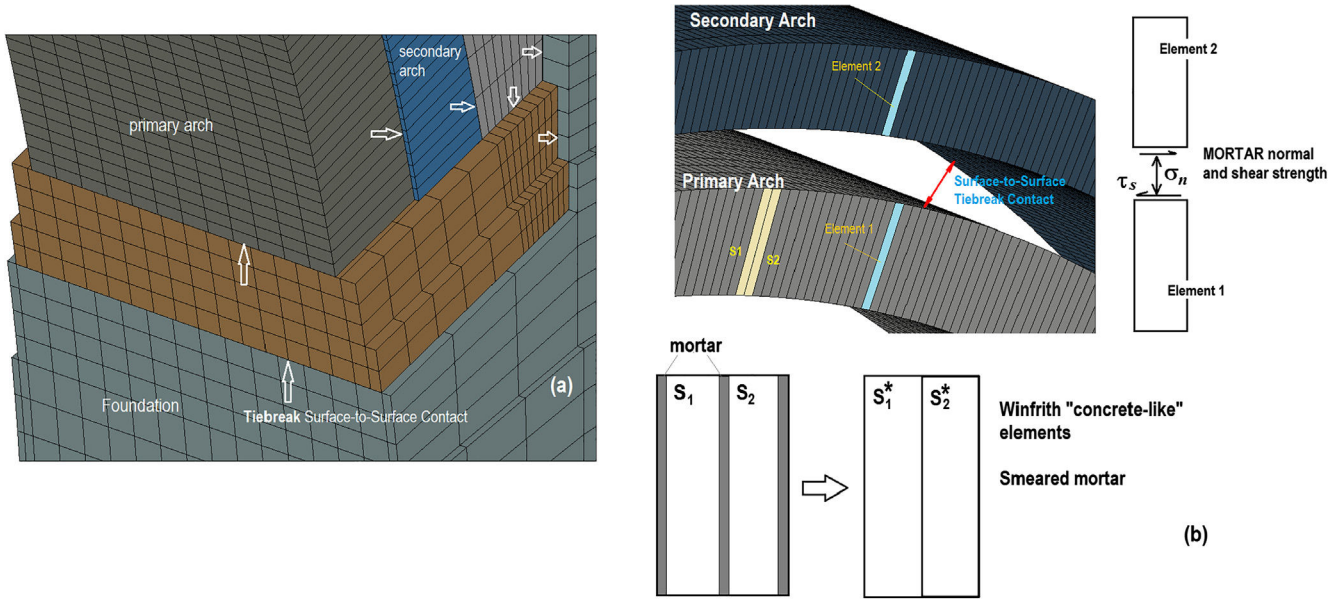

Fig. 6. Implementation of (a) "discontinuous" and (b) "continuous" strategies in capturing the interaction between bridge structural sections.

formulated within the LS-DYNA code (***Tiebreak_surface_to_surface***) and enabling the separation of two surfaces in contact when failure criteria are met has been adopted. Normal to the interface stresses and shear stresses form the failure envelope governed by the relation,

$$\left[\frac{|\sigma_n|}{\sigma_{fail}}\right]^2 + \left[\frac{|\tau_s|}{\tau_{fail}}\right]^2 \geq 1 \quad (1)$$

With σ_n and τ_s being the normal and shear stresses of the interface between segments of the structure. σ_{fail} is the tensile failure stress and τ_{fail} is the shear failure stresses of the mortar assumed to be present between the structural sections in surface-to-surface contact. Fig. 6b depicts an exploded view of the surface-to-surface interface between the upper surface of the primary arch and the lower face of the secondary arch. The failure stresses are deduced from laboratory tests. Following failure at the interface the structural segments will remain in contact acted upon compressive loads and will move apart under tensile loads. After failure no interface tension is possible. The laboratory tests conducted as part of this study deduced only compressive and tensile strengths of the representative mortar. As a result, based on the test data from both this and other studies [11], the mortar shear strength was assumed to be equal to the tensile strength deduced from flexure tests (1.267 MPa). The normal mortar strength for interface failure was assumed in the numerical analyses to be as low as 0.42 MPa and up to 1.26 MPa for tensile crack initiation. It should be pointed out that these assumed tensile strength values of mortar, in particular, are accompanied with significant uncertainty due to the limited test specimens allowed to be removed from the collapsed bridge.

Within each structural section the discretization is "continuous" where elements or "units" represent the two-phase material (stone and mortar). The bond between the stone and mortar is deemed to be the weakest link in the stone masonry system and so the stone-mortar interface is most relevant.

The aim is, instead of adopting a complete micro-model that include all the failure mechanisms of masonry, such as, cracking at the interface of stone and mortar, cracking and crushing of stones, to create a homogenized unit where both constituents contribute to the state of stress and failure. Fig. 6b depicts the transformation of the two-phase material into a homogeneous unit. To capture the "weakest" link in the homogenous unit (i.e. tensile cracking in the mortar) it is assumed that failure in tension to be controlled by the mortar and failure under compression (crushing) by the stone part. To achieve such a representation of the constitutive behavior of the stone-mortar homogeneous unit or element the Winftrith concrete-like constitutive relations [44] and behavior was implemented. In such material the stone represents the concrete and the mortar the reinforcement. The mortar is assumed to be smeared within the homogeneous unit. According to the approach stresses for the two constituents are computed separately and the two components are smeared together according to their relative cross-sectional areas to form the total element stress. An elastic, perfectly plastic behavior is assumed for the mortar. Tensile and compressive stresses deduced from the laboratory tests summarized in Section 3.2 are used for the non-linear behavior with a ratio of mortar to stone varying from structural section to section (smallest in the discretization of the two arches of 5%). Threshold tensile stress for crack initiation was assumed 1.26 MPa (tensile strength of mortar from flexure tests). Upon formation of a tension crack no tensile load can be transferred across the crack faces. Fracture energy $\boldsymbol{G_f} = 80$ N/m dissipated in the opening of a tension crack was assumed. $\boldsymbol{G_f}$ is defined as the amount of energy to create a crack of unit area. For the actual stone-mortar system that would occur along the stone-mortar interface but for the homogeneous element adopted here it can occur with any orientation within the element. To define the failure of mortar failure tests were conducted on small masonry specimens [9,10] leading to $\boldsymbol{G_f}$ values ranging from 5 to 20 N/m for tensile bond strengths in the range of 0.3–0.9 MPa. Higher $\boldsymbol{G_f}$ values (up to 250 N/m) were deduced for failure in shear. Compressive failure of the homogeneous unit (crushing), Winfrith concrete-like material is considered to be controlled by the stone strength. The hydrostatic component of the stone stress field is computed from the form,

$$P_i = \frac{\sigma_c}{3} \qquad K = \frac{\mathrm{Es}}{3(1-2\nu)} \quad (2)$$

P_i is the pressure at uniaxial compressive failure of the stone, K is its bulk unloading modulus, E_s is the tangent modulus and ν is the Poisson's ratio. The critical pressure *Pi* deduced from the compressive stone strength σ_c is used in the present analysis to trigger crushing in a given unit and consequently its elimination (erosion) from the structure.

3.3. Model calibration based on measured modal characteristics

The bridge was modeled using four different materials reflecting

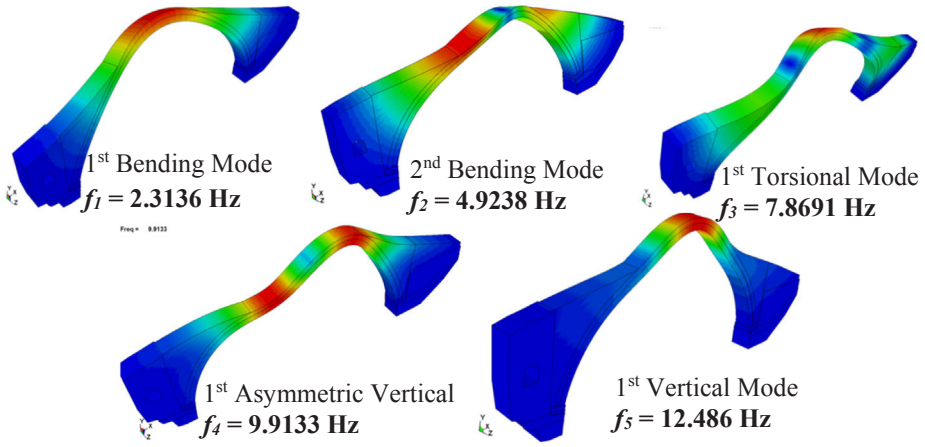

Fig. 7. Predicted Konitsa Bridge modes using the 3-D "pseudo-linear" model.

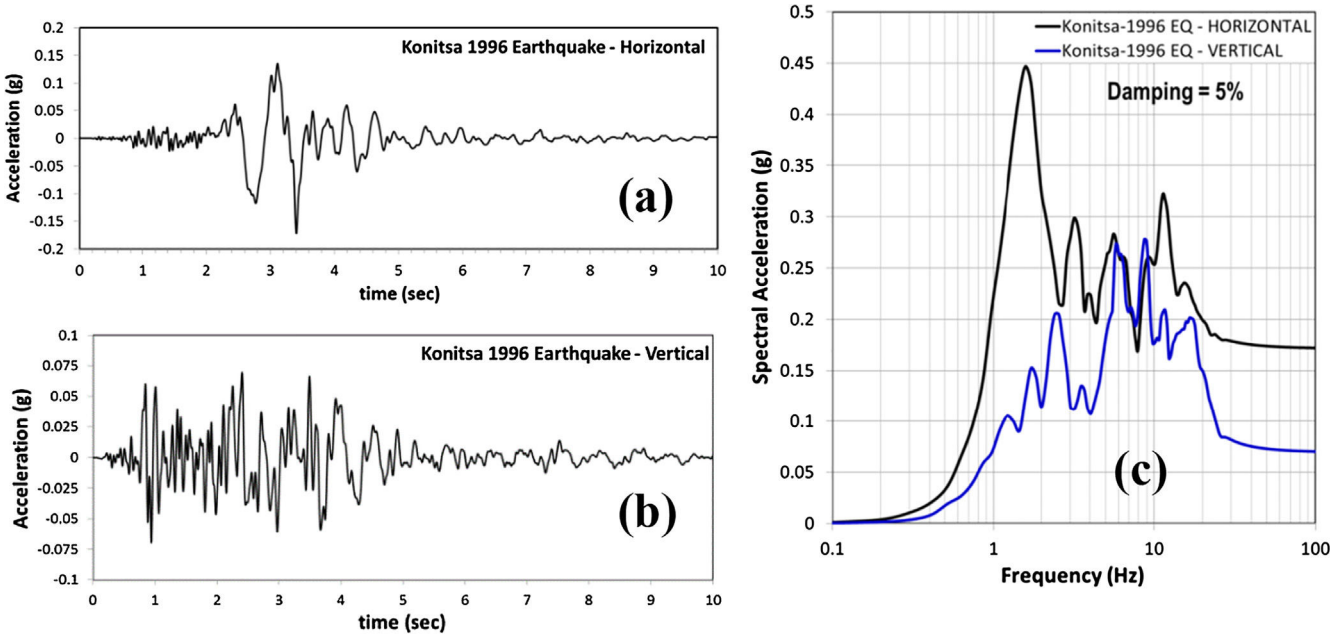

Fig. 8. Konitsa 1996 earthquake acceleration recordings (~1.5 Km from bridge) on hard rock formation, (a) horizontal and (b) vertical. (c) 5% response spectra.

differences in both the stone quality and percent mortar for different sections using a total of 72,540 solid, one-point integration elements. In addition, a total of fourteen interfaces with tiebreak failure criteria controlled by the mortar shear and tensile strength were incorporated to capture the interaction between distinct structural sections.

The model was assumed to be fixed on competent rock on both sides and therefore no Soil-Structure-Interaction (SSI) effects were considered. The LHS abutment of the actual bridge is supported on competent rock. The RHS abutment on the other hand appears to be supported by weathered rock. For this study, and in the absence of geotechnical and foundation depth and construction information and/or details regarding the RHS abutment, it has been assumed that both abutments are on competent rock. The fundamental modes of the idealized structure were deduced using the "pseudo-linear" equivalent of the 3D non-linear numerical model whose properties and constitutive relations were described above with isotropic elastic material behavior (density $\rho = 2.69$ g/cc, $E = 17$ GPa, $\nu = 0.21$). Fig. 7 depicts modal frequencies and shapes predicted by the numerical eigen analysis. It can be observed that while the out-of-plane primary modes are in good agreement with those identified from measured data from the two independent field studies, deviations exist in the in-plane modes. As noted above this is attributed to the anisotropy that inherently exists in the global stiffness of the bridge (out-of-plane vs. in-plane) compounded by the inherent error of degrading the fully non-linear model with "discontinuous" discretization between structural sections to an equivalent linear one. The agreement, however, between predicted and measured modes is considered sufficiently satisfactory for the bridge earthquake response.

4. Near-field and far-field earthquake response and bridge damage

The seismic response and vulnerability of the case study bridge was conducted based on the 3D non-linear model developed and reflecting (a) the material properties deduced from the laboratory tests and (b) the constitutive and failure envelope relations discussed in Section 3. The primary objective is to observe the sensitivity of the bridge response and induced damage to different types of earthquakes, i.e. near-field and far field. To arrive at an assessment real earthquake records the exhibit the near-field and far-field characteristics were utilized.

As a baseline analysis, the earthquake recording obtained during the 1996 event approximately 1 Km distance away from the LHS abutment

of the Konitsa Bridge was used to obtain the response and damage potential. As noted previously, no earthquake recording is available on the actual structure. The 0.19 g peak ground acceleration record on the same rock formation, however, represents a close approximation to the actual seismic excitation. Furthermore, the assessment of damage to the structure following the earthquake offers a good basis for comparing the actual performance with the simulation results. The recorded ground motions on rock (~1 Km away from the bridge) are shown in Fig. 8a–b [25]. The strong motion acceleration exhibits the characteristics of an impulse-type or near-field earthquake (NFE) especially in its horizontal component which contains the characteristic pulse of a near-field earthquake. The 5% response spectra of the recorded accelerations are also shown in Fig. 8c. Damping ratios deduced from the field studies (1.7–2.7%) were used in the seismic analysis.

The baseline analysis of the Konitsa Bridge revealed the following:

- The bridge static analysis performed as a pseudo-dynamic analysis with fictitiously high global damping and the onset of gravity as the dynamic excitation confirmed that the entire structure is in compressive state throughout, free of damage and tension cracks.
- Uniform, three-dimensional excitation of the bridge applied at the LHS and RHS abutments with in-plane and out-of-plane horizontal components considered identical and no SSI considerations (assumed both be fixed on rock) resulted in (a) no interface separation between distinct structural sections of the bridge assumed in the analysis to be controlled by the mortar strength in tension and shear and (b) only limited micro-cracking is predicted by the analysis near the support locations of the main arch. These predictions on structural damage are in-line with the in-situ observations and inspection made following the actual earthquake event of 1996 [21] where only limited damage to parapet sections, spalling of the concrete cover placed in the intrados of the main arch during restoration work in the 1980s and few tension cracks near the RHS foundation were observed (see Fig. 9).

The sensitivity to the earthquake type of this large arch stone bridge (representing the class of such structures), following the validation of its dynamic characteristics and the earthquake analysis which predicted no extensive damage (as also observed) was performed using the following four real earthquake signals which represent near-field and far-field characteristics:

(a) The NS component observed at Shiofukizaki site in the 1989 Ito-oki earthquake of moment earthquake magnitude 5.3, epicentral distance of 3 km, and the depth of the seismic source of 5 km. The record was observed at the surface of basalt rock and has a maximum acceleration of 0.189 g. It has been characterized as a near-field earthquake.

(b) The EW component of an earthquake observed at the Kashyo Dam site during the 2000 Tottori-ken Seibu earthquake of moment magnitude 6.6 with epicentral distance of 3 km, seismic source depth of 11 km and maximum acceleration of 0.531 g. Kashyo Dam earthquake characterized as near-field.

(c) The 1957 San Francisco-Golden Gate Park far-field earthquake of 5.3 magnitude, focal distance of 18 Km and peak acceleration of 118 cm/s^2, peak ground velocity of 4.6 cm/s normalized for this study to 0.531 g to match the PGA of the Kashyo Dam earthquake

(d) The 1940 El Centro (far-field) earthquake normalized to 0.19 g to enable comparison with the similar PGA Konitsa 1996 and Ito-Oki near-field earthquakes

The recorded acceleration traces of these four earthquakes are shown in Fig. 10 and the associated response spectra in Fig. 11. Peak ground acceleration, peak ground velocity (PGV), Response and power spectra as well as cumulative absolute velocity (CAV) and Arias intensity (I_A) were computed and utilized to interpret the results of the dynamic analyses and correlate damageability of these earthquakes (based on widely used criteria deduced from their intensity and spectral characteristics) with the damage potential predicted for the stone bridge of this type. The CAV and I_A parameters used in the analysis are computed based on Eq. (3) shown below.

$$\mathbf{CAV} = \int_0^{t*} |\alpha(t)|\, dt \quad \text{and} \quad \boldsymbol{IA} = \frac{\pi}{2g} \int_0^{t*} \alpha^2(t) dt \tag{3}$$

Fig. 12 compares the predicted damage of the Konitsa Bridge from the near-field 0.189 g Ito-Oki and the normalized to 0.19 g far-field El Centro earthquakes. Similar response and limited damage to the one observed in the Konitsa 1996 earthquake study is predicted for the near-field Ito-Oki earthquake (Fig. 12a). It is assessed that the similarity in response/damage observed to be the result of the type of earthquake (impulsive, near field) rather than the similarity in peak ground acceleration (0.19 g vs. 0.189 g). This assessment is reinforced by the analysis/damage results deduced using as seismic excitation the El Centro far-field type earthquake with peak ground acceleration normalized to 0.19 g. As shown in Fig. 12b, a dramatically different response and damage is observed when compared to the Ito-Oki and Konitsa 1996 near-field type earthquakes. Examination of induced global deformation revealed that while the Ito-Oki and Konitsa 1996 earthquakes excited primarily the first symmetric (out-of-plane) mode, the El Centro earthquake appeared to also excite the asymmetric out-of-plane modes of the bridge.

To further scrutinize and validate the dramatic differences observed in the response and damage depending on the characteristics of the earthquake (near vs. far field) at even higher peak ground accelerations, the Kashyo Dam (0.54 g) near-field and San Francisco-Golden Gate Park (0.53 g) far-field earthquakes were used to excite the structure. Fig. 13

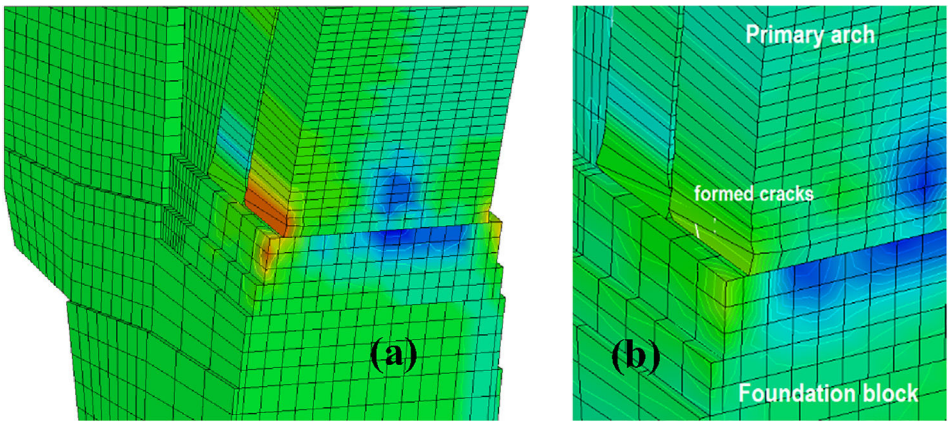

Fig. 9. Predicted stress profile during earthquake excitation (a) and tension crack development (b) in the Konitsa Bridge during the 1996 0.19 g earthquake.

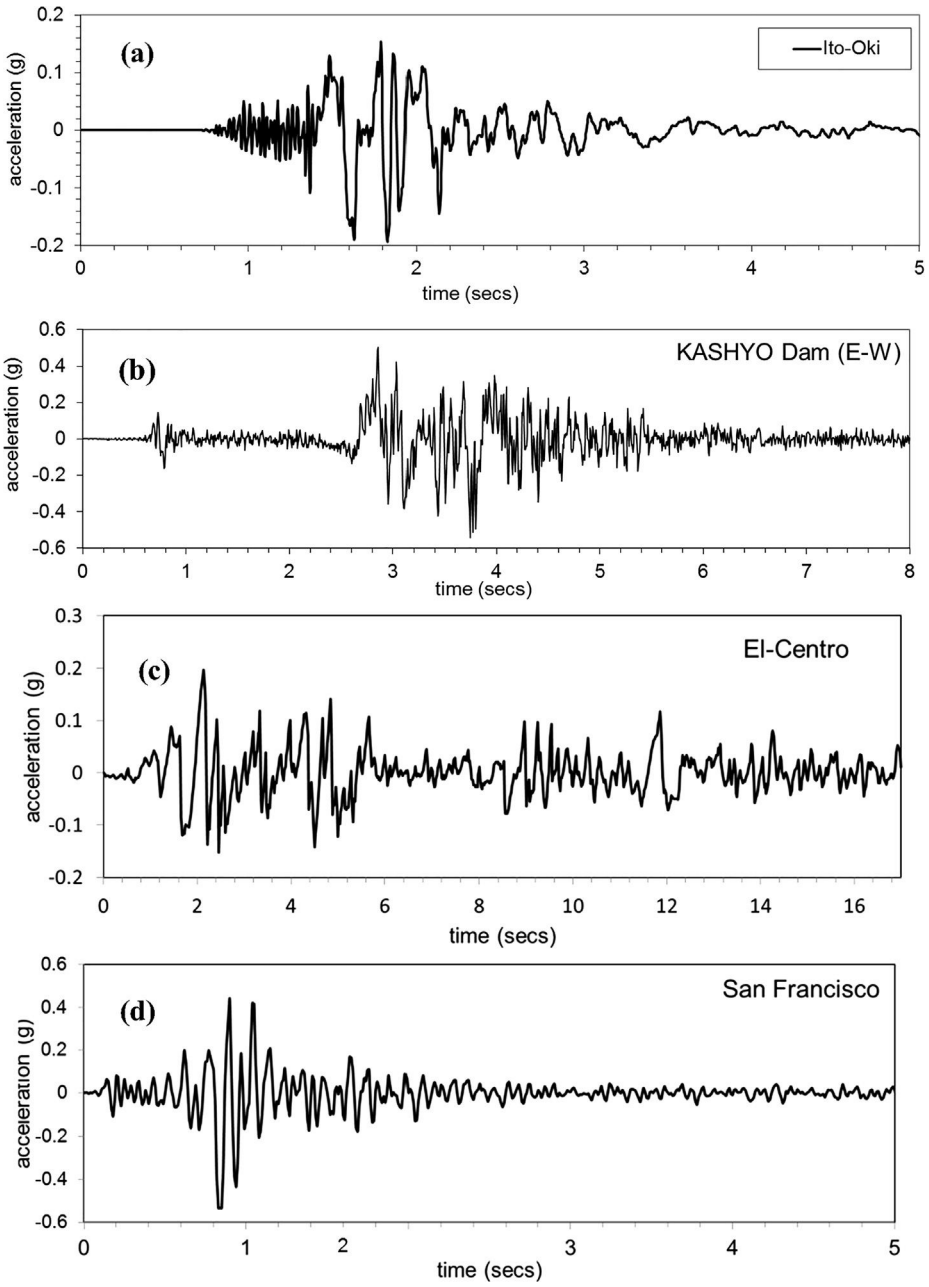

Fig. 10. Acceleration time histories of the four (4) actual earthquakes used in the study of the Konitsa Bridge seismic vulnerability (a: Ito-Oki, b: Kashyo Dam, c: El Centro and d: San Francisco).

depicts damage resulting from these higher PGA earthquakes. In Fig. 13a the near-field Kashyo Dam earthquake only causes tension cracks at the bridge crown but no collapse. Contrary, as seen in Fig. 13b the damage of the Konitsa Bridge from the similar PGA far-field San Francisco (0.53 g) earthquake is predicted by the same analysis to result in extensive damage and subsequent collapse. These results of higher damageability of the far-field earthquakes on this type of stone masonry bridges agree with findings of experimental studies on nuclear structures [29–31] of the less damaging effects induced by near-field earthquakes.

To help explain the predicted dramatic difference of earthquake damage potential for this type of structures (large stone arch bridges) the CAV and I_A damage indicators of the studied earthquakes are evaluated. Specifically, the CAV values of the earthquakes utilized in the vulnerability analysis computed according to Eq. (3) are listed below.

$CAV_{Konitsa\text{-}H}$ (*0.19* g) = 0.150 g s	$CAV_{Konitsa\text{-}V}$ (*0.12* g) = 0.113 g s
$CAV_{Ito\text{-}Oki}$ (*0.19* g) = 0.188 g s	$CAV_{El\ Centro}$ (*0.19* g) = 0.348 g s
$CAV_{Kashyo\text{-}Dam}$ (*0.54* g) = 0.531 g s	$CAV_{San\ Francisco}$ (*0.53* g) = 0.223 g s

In correlating the damage observed with the CAV computed for each earthquake is assessed by the authors that the CAV damage metric can adequately explain the bridge response differences between the low PGA earthquakes (Konitsa 1996, Ito-Oki and El Centro). The CAV metric, however, fails to correlate the damage observed under the action of the higher PGA earthquakes (Kashyo-Dam and San Francisco).

The Arias intensities, as alternative damage indicators, of the studied earthquakes have been computed and are depicted in Fig. 14. Similarly, with the CAV damage indicator, the I_A correlates well with the predicted damageability for low PGA earthquakes (Fig. 14a) but deviates at the higher PGA (Fig. 14b) with predicted damage. Using the I_A

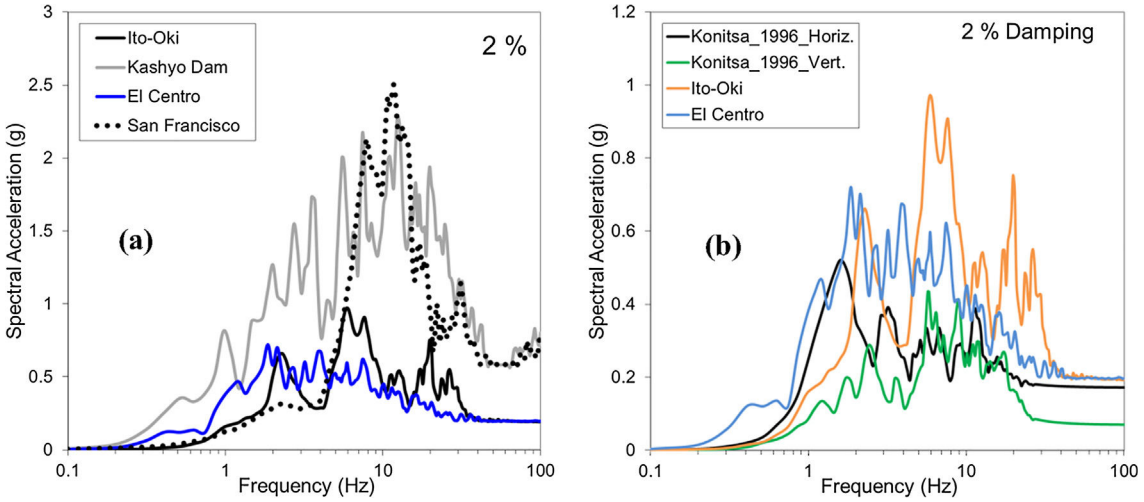

Fig. 11. (a) 2% acceleration response spectra of the four earthquakes and (b) 2% response spectra of the Konitsa 1996 earthquake comparison with the near-field Ito-Oki and El Centro far-field earthquakes.

measure depicted in Fig. 14 and the rate parameter introduced by Trifunac [32] a different approach to correlating damage predicted with input earthquake indicators is explored. According to [32], and for both linear domain with viscous damping or nonlinear ranges of structural response, a structure is capable of dissipating only a certain amount of vibrational energy per unit time. If the dissipation rate is higher than the rate of the input seismic energy the structure may survive a particular excitation. Conversely, if the input rate is higher than that of dissipation, then the structure is expected to experience permanent progressive damage to create a higher energy dissipation capacity, and for prolonged shaking it would eventually collapse. Such input rate is defined in terms of earthquake acceleration, velocity and ground displacement according to Eq. (4).

$$\text{Rate}^{\alpha} = \frac{1}{T_{2-T_1}}\int_0^{\infty}\alpha^2(t)dt;\ \text{Rate}^{v} = \frac{1}{T_{2-T_1}}\int_0^{\infty}v^2(t)dt;\ \text{Rate}^{d} = \frac{1}{T_{2-T_1}}\int_0^{\infty}d^2(t)dt \tag{4}$$

where T_1 and T_2 enclose the 5% and 95% of the integrated quantity (mean-square value of $\alpha(t)$, $v(t)$ or $d(t)$ evaluated over the entire earthquake duration. The shown integrals define average rate at which the seismic-wave energy passes by a recording station. Analysis based on the energy rate depicted above was performed for all earthquakes examined with particular focus on the higher PGA earthquakes (Kashyo Dam and San Francisco). The comparison revealed that all indicators associated with the Kashyo Dam 0.54 g near-field earthquake are higher than those linked with the 0.53 g San-Francisco earthquake. The differences, however, in the value of the metrics are significantly reduced as compared with the CAV and IA indicators (Rate$^{\alpha}$ Kashyo Dam = 40.0 m/s vs. 35.0 for the San Francisco earthquake).

Based on these findings on damage prediction (via 3D, non-linear analyses) and its correlation with strong motion shaking as well as earthquake damageability indicators (CAV, $\mathbf{I_A}$ and Rate) developed over the years and widely applied to nuclear structures, it is assessed by the authors that stone arch bridges represent a unique, a-typical class of structures where a combination of damage indicators might be needed

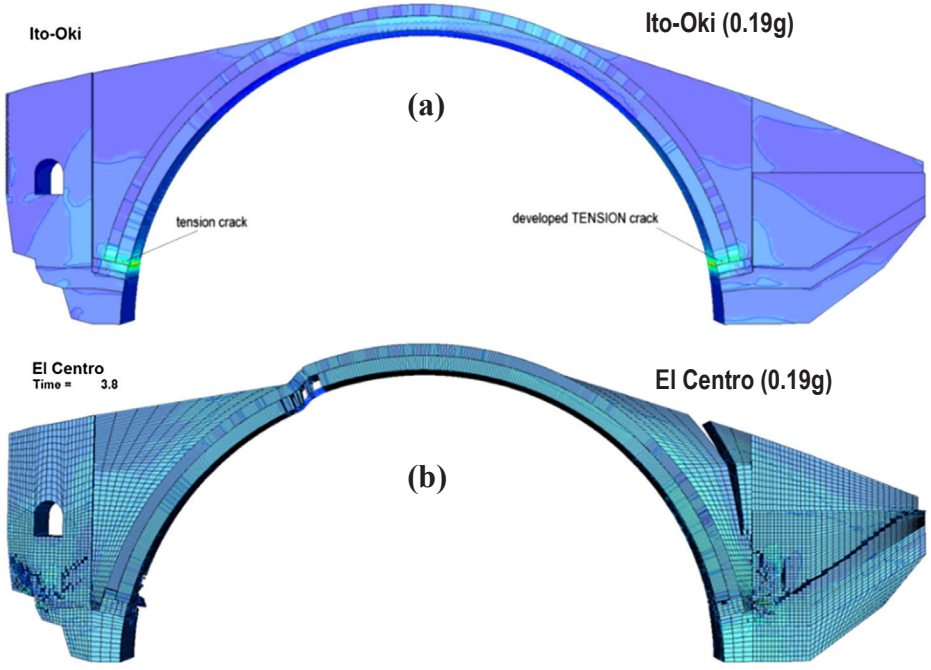

Fig. 12. Predicted damage resulting from similar PGA earthquakes, (a) 0.19 g Ito-Oki and (b) El Centro normalized at 0.19 g.

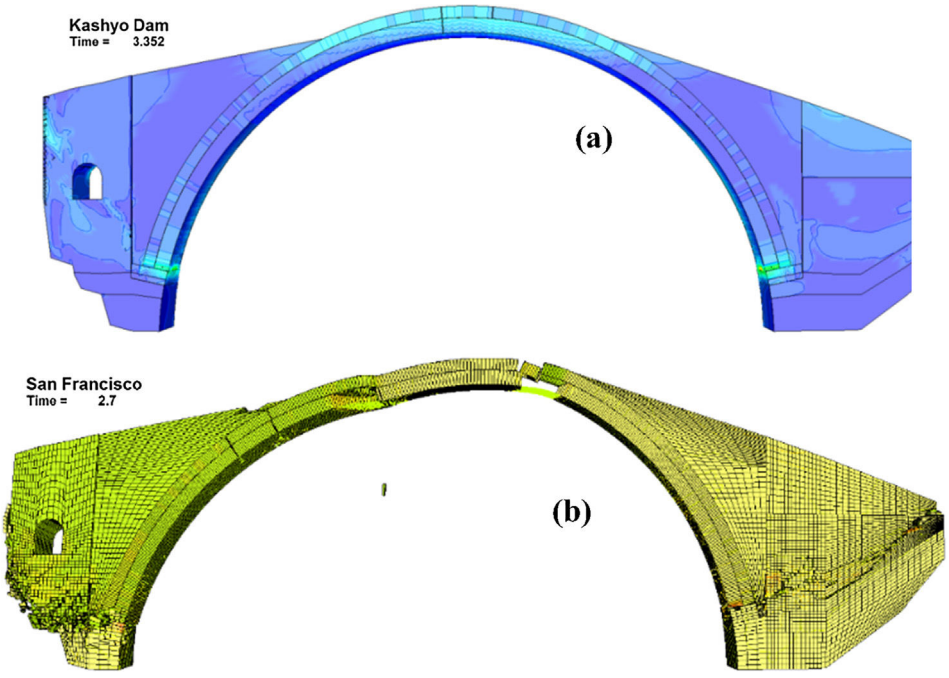

Fig. 13. Comparison of predicted damage in Konitsa Bridge subjected to (a) near-field Kashyo Dam (0.54 g) and (b) far-field San Francisco (0.53 g) earthquakes.

to predict earthquake-induced damage when higher PGA values are involved.

5. Summary and conclusions

The earthquake-induced damage on a large stone arch bridge (Konitsa Bridge) used as a case study representing a family of such structures found in earthquake-prone zones has been studied with particular focus on the sensitivity of damage to the near-field and far-field type of earthquakes.

Selection of the case study bridge was prompted by the fact that the said bridge is located on a known, active fault, has experienced an impulse-type or near field earthquake of ~0.19 g in 1996 and survived with no damage and finally, actual earthquake recordings on the same rock formation at ~1 Km distance from the bridge have been made. Furthermore, the recent collapse due to flooding of a similar, but even larger stone arch bridge, constructed with the same techniques, around the same period and with similar structural materials, has made the need of seismic vulnerability more urgent.

Two independent field studies were conducted to establish the dynamic characteristics of the case study bridge and help calibrate the 3D non-linear analysis model developed to study the earthquake response and predict damage. Laboratory tests on stone and mortar specimens from the recently collapsed Plaka Bridge, which are expected to represent the material properties of the case study bridge, provided realistic mechanical strength and property values for the constitutive models implemented in the earthquake analyses. The constitutive and failure relations implemented in the study have been used in the simulation of the collapse of similar bridge leading to a very satisfactory prediction of its collapse [19].

In addition to the ground motion recordings of the 1996 Konitsa near-field earthquake, four additional earthquakes (two with the characteristics of near field and two those of a far field) were introduced and their damageability was compared. The study revealed the following:

Far-field earthquakes were shown to be far more destructive than their near-field counterparts. This important finding deduced from the present study on this type of tone structures is in excellent agreement with the conclusion that has been reached for nuclear structures following a series shake table experiments and assessment [29–31] as well

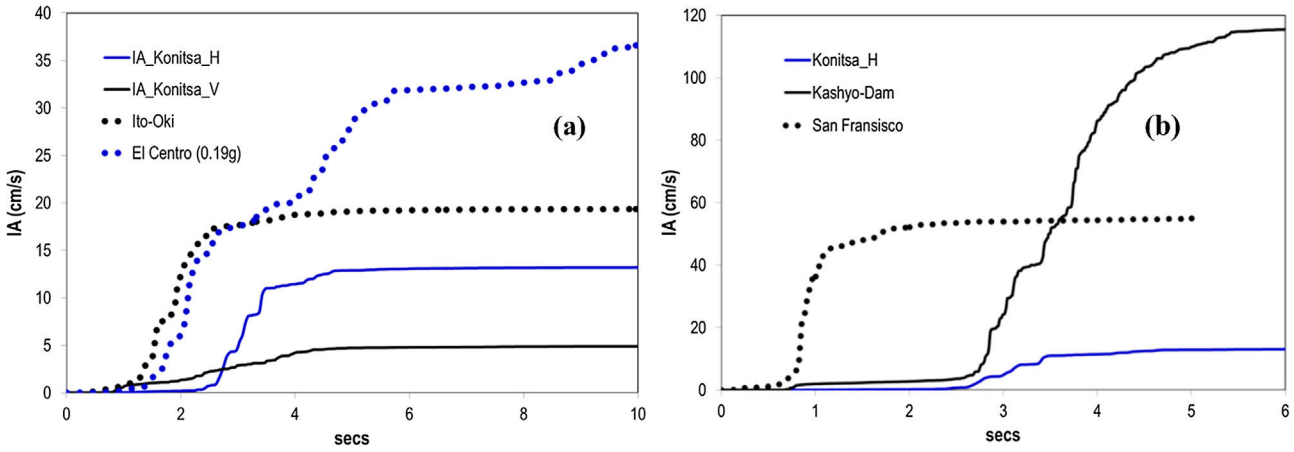

Fig. 14. Computed Arias intensities (IA) for the examined earthquakes. (a) lower PGA (~0.19 g) earthquakes and (b) higher PGA (~0.54 g) earthquakes.

as the decades-long practice of sitting nuclear facilities in the proximity of faults capable of producing earthquakes of magnitude M ≤ 5.5 due to their low damage potential [29]. Studies based on elastic-linear response of similar stone bridges [8], and without accounting for the progressive damage induced, have indicated that the elastic response (not damage) of such structures may be higher under near-field earthquakes than the far-field counterparts, a response that stems from the characteristic dominant velocity pulse of the n

Earthquake damage indicators such as CAV, Arial Intensity I_A and energy rate, developed over the years to comparatively assess damage to conventional or nuclear structures, correlated well with the damage predicted using the 3D non-linear analyses of the case study bridge al low earthquake PGA values but deviated significantly at higher PGA. It is the opinion of the authors, given the structural shape of these bridge structures, the materials used in their construction, including weathering, all influencing their dynamic characteristics, that a combination of these damage indicators may be needed for vulnerability assessment.

References

[1] Aoki T. et al. Theoretical and experimental dynamic analysis of Rakanji stone arch bridge, Honyabakei, Oita, Japan. In: 7th Int. conference on motion and vibration control, MOvIC 04; 2004.

[2] Kiyono J. et al. Seismic assessment of stone arched bridges. In: Proceedings, 15 WCEE, Lisboa, Portugal; 2012.

[3] Castellazzi G, De Miranda S, Mazzotti C. Finite element modelling tuned on experimental testing for the structural health assessment of an ancient masonry arch bridge. Math Probl Eng 2012;2012:495019.

[4] Lourenço PJBB. Computational strategies for masonry structures. PhD Thesis: Delft University Press; 1996.

[5] Pelà L, Aprile A, Benedetti A. Seismic assessment of masonry arch bridges. Eng Struct 2009;31:1777–88.

[6] Rovithis EN, Pitilakis KD. Seismic assessment and retrofitting measures of a historic stone masonry bridge. Earthq Struct 2016;10(3):645–67.

[7] Sevim B, et al. Finite element model calibration effects on the earthquake response of masonry arch bridges. Finite Elem Anal Des 2011;47:621–34.

[8] Sevim B, et al. Ambient vibration testing and seismic behavior of historical arch bridges under near and far fault ground motions. Bull Earthq Eng January 2016;14(1):241–59.

[9] Pluijm, van der, R. Material properties of masonry and its components under tension and shear. In: w Proceedings 6th Canadian masonry symposium, Saskatoon, Canada; 1992. p. 675–86.

[10] Pluijm, van der R. Shear behavior of bed joints. Proc. 6th North American masonry conf. Philadelphia, Pennsylvania, USA: Drexel University; 1993. p. 125–36.

[11] Cavicchi A, Gambarotta L. Collapse analysis of masonry bridges taking into account arch–fill interaction. Eng Struct 2005;27:605–15.

[12] Silva B. et al. Calibration of a numerical material behavior model for the simulation of multi-leaf stone masonry walls. In: Proceedings of 8th international conference on structural analysis of historical constructions (SAHC); 2012.

[13] Drosopoulos GA, et al. Limit analysis of a single span masonry bridge with unilateral frictional contact interfaces. Eng Struct 2006;28:1864–73.

[14] Pugi F. Seismic analysis of masonry arch structures through finite element model "Block-Joint". In: COMPDYN; 2013.

[15] Tarque N. et al. Numerical modeling of the in-plane behavior of rubble stone masonry. In: Proceedings of 9th international conference on structural analysis of historical constructions; 2014.

[16] Caglayan BO, et al. Assessment of a concrete arch bridge using static and dynamic load tests. Struct Eng Mech 2012;41(1):83–94.

[17] Roca Pere, et al. Structural analysis of masonry historical constructions. classical and advanced approaches. Arch Comput. Methods Eng 2010;17:299–325.

[18] Simos N, Manos GC. Numerical analysis of seismic response of natural stone arch bridges – field observations and a case study. In: COMPDYN; 2013. http://www.eccomasproceedings.org/cs2013/.

[19] Simos N. et al. On the assessment of the plaka bridge collapse using non-linear analysis – preventable or doomed?. In: Eccomas Procedia COMPDYN; 2017. p. 423–40.

[20] Manos GC, Simos N, Kozikopoulos E. The structural performance of stone masonry bridges in Greece. Structural bridge engineering In-Tech Publishing; 2016. https://doi.org/10.5772/64752.

[21] Korompilias D. Μελέτη ανελαστικής συμπεριφοράς του γεφυριού της Κόνιτσας με χρήση ανελαστικού προσομοιώματος για τοιχοποιία και εφαρμογή μεθόδων ενίσχυσης. PhD Thesis. University of Patras, Greece (in Greek); 2015.

[22] Papanastasiou et al. The Konitsa, Epirus NW Greece, July 26 (Ms = 5.4) and, (Ms = 5.7) earthquakes sequence. Bull. Geol. Soc. Greece, XXXIV, 1555–1562; August 5, 1996.

[23] Galanakis D. et al. Neotectonic activity of Konitsa Area and the Earthquakes; 1996. http://www.hellenjgeosci.geol.uoa.gr/42/57-64.pdf.

[24] Spyrakos CC, et al. Evaluation of near-source seismic records based on damage potential parameters case study Greece. Soil Dyn Earthquake Eng 2008;28:738–53.

[25] Institute of Engineering Seismology and Earthquake Engineering (ITSAK). Data Base of Greek Earthquake Strong Motions.

[26] Provisions of Greek Seismic Code 2000. OASP, Athens, December 1999. Revisions of seismic zonation introduced in 2003.

[27] Euro-Code 8 – Design of structures for earthquake resistance – Part 2 Bridges: DRAFT No 3. European Committee for Standardization; 2004.

[28] Paz M. International handbook of earthquake engineering: codes, programs and examples. Mario Paz, Greece by Manos GC, (editors), Chapman and Hall, ISBN 0-412-98211-0; 1994 [chapter 17].

[29] Non-linear Response to a Type of Seismic Input Motion, IAEA-TECDOC-1655-ISSN 1011-4289; 2011.

[30] Labbé P, Altinyollar A. Conclusions of the IAEA-JRC research project on the safety Significance of near-field earthquakes. Nucl Eng Des 2011;241:1842–56.

[31] Simos N. et al. Experimental studies of reinforced concrete structures under multi-directional earthquakes and design implications. NUREG/CR-7119; 2013.

[32] Trifunac MD, Brady AG. A study on the duration of strong earthquake ground motion. Bull Seismol Soc Am June 1975;65(3):581–626.

[33] Bradley BA. Ground Motion Comparison of the 2011 Tohoku, Japan and 2010–2011 Canterbury earthquakes: Implications for large events in New Zealand. Paper Number 039, 2012 NZSEE Conference; 2012.

[34] Manos GC. Consequences on the urban environment in Greece related to the recent intense earthquake activity. Int J Civil Eng Architec 2011;5(12):1065–90. Serial No. 49.

[35] Manos GC, et al. Field experiments for monitoring the dynamic soil-structure-foundation response of model structures at a Test Site. J Struct Eng Am Soc Civil Eng 2015;141(1) [Special Issue "Field Testing of Bridges and Buildings, D4014012].

[36] Manos GC, Kozikopoulos E. In-situ measured dynamic response of the bell tower of Agios Gerasimos in Lixouri, Kefalonia, Greece and its utilization of the numerical predictions of its earthquake response. In: COMPDYN 2015, Greece; 25–27 May 2015.

[37] Manos GC, Kozikopoulos E. The dynamic and earthquake response of Basilica Churches in Kefalonia, Greece including soil-foundation deformability and wall detachment. In: COMPDYN 2015, Greece; 25–27 May 2015.

[38] Manos G.C. et al. Numerical simulation of the limit non-linear behaviour of unreinforced masonry under in-plane state of stress from gravitational and seismic actions. In: COMPDYN 2015, Greece; 25–27 May 2015.

[39] Colin O'Connor. Roman bridges. Cambridge University Press; 1993. ISBN 0-521-39326-4.

[40] Biolzi L, Catanneo S, Rosati G. Flexural/tensile strength ratio in rock-like materials. Rock Mech Rock Eng 2001;34(3):217–33.

[41] The stone masonry arch bridges of Greece, Center of environmental education Makrinitsas. ISBN: 978-960-98043-9-4, (in Greek); 2007. http://kpe-makrin.mag.sch.gr.

[42] Psimarni K. et al. Development of a Geographic Information System for the Traditional Bridges of Central Zagori. Report to the Municipality of Zagori (in Greek); 2000.

[43] Simos N, Manos GC. Structural integrity assessment of historical stone structures based on passive monitoring of their dynamic characteristics. (in preparation).

[44] Hallquist JO. LS-DYNA. Keyword User's Manual. Version 971. Livermore: Livermore Software Technology Corporation; 2007.

[45] TrueGrid – Version 2.3.4, XYZ Scientific Applications, Inc; 2015.